euspen's 21st International Conference & Exhibition, Copenhagen, DK, June 2021
www.euspen.eu

Methodological correlation of finite element models to nanoindentation measurements on Si (100)

Jelena Srnec Novak,[1, 2] Ervin Kamenar,[1] Saša Zelenika,[1] Francesco De Bona [2] and Laura Piovesana [2]

[1] *University of Rijeka, Faculty of Engineering & Centre for Micro- and Nanosciences and Technologies, Vukovarska 58, 51000 Rijeka, Croatia*
[2] *Polytechnic Department of Engineering and Architecture, University of Udine, Via delle Scienze 206, 33100 Udine, Italy*

jsrnecnovak@riteh.hr

Abstract
A viable approach to obtain mechanical properties such as Young's modulus and hardness, is testing on a nanoindentation device. Such an experimental procedure can, however, be time-consuming and expensive. Finite element analysis (FEA) can be employed to minimize the number of required measurements, i.e., to obtain numerically the load vs. indentation depth curves for varying input parameters, hence extracting the resulting elasto-plastic material properties. A methodological approach is used in this work to correlate the responses obtained via FEA to nanoindentation experimental data. A (100)-oriented single crystal silicon wafer is used as a testing sample. Numerical simulations are performed by employing a bilinear elasto-plastic material model. A sensitivity analysis of the characteristic parameters of the material model is then conducted on the numerically obtained load vs. displacement curves. The proposed methodology enables replicating the experimental curves with estimated errors lower than 1 % and 15 % for Young's modulus and hardness, respectively. The performed analyses allow establishing also that, when evaluating numerically hardness, the tip radius and shape significantly affect the accuracy of the results, especially for lower indentation depths.

Nanoindentation, FEA numerical calculations, elasto-plastic material model, correlation methodology, MEMS and NEMS

1. Introduction

The most common use of nanoindentation is in establishing mechanical properties such as hardness and Young's modulus. Recently there has been a significant progress in measuring also other mechanical parameters, such as the hardening exponent, creep parameters, or the residual stresses [1]. Nanoindentation measurements are, however, often expensive and time-consuming so that, to minimize the number of tests, finite element analysis (FEA) can be applied. In fact, it was established that, while one experiment lasts a few minutes (even without considering preparation) a single FE simulation provides results within one minute. What is more, FEA can be used as a virtual tool to investigate the features of the nanoindentation test that are not directly available from experimental characterization [2]. FEA allows thus obtaining numerically the load (*P*) vs. indentation depth (*h*) curves for varying input parameters, hence attaining the resulting elasto-plastic material properties [3].

A methodological approach is followed in this work to correlate the responses obtained via FEA to nanoindentation experimental data. Measurements on a (100)-oriented single crystal silicon (Si) wafer are performed by using a nanoindentation device, while adopting the standard depth-controlled loading-unloading method and varying the indentation depths. Numerical simulations are, in turn, performed by employing in a first instance a nonlinear FEA with elastic material behaviour, optimized in terms of the characteristic dimensions of the numerical model. Once the optimal geometrical parameters are defined, numerical simulations with an elasto-plastic material model are carried on. A sensitivity analysis of the characteristic parameters of the material model is finally conducted on the numerically obtained *P-h* curves.

2. Materials and methods

Nanoindentation is a viable method to determine the indentation hardness (*H*) and Young's moduli (*E*) by performing automated tests. During the nanoindentation tests, the tip of the indenter is pressed into the sample material in a prescribed loading and unloading set-up, while *P* and *h* are concurrently recorded in the form of a load vs. displacement curve.

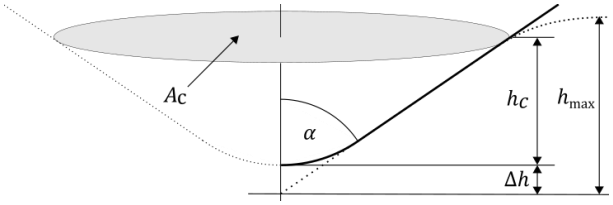

Figure 1. Theoretical and corrected geometry of an indenter tip.

The main difference between conventional hardness and nanoindentation tests is the approach followed to obtain the contact area between the tip and the sample. In fact, while in conventional tests the contact area is measured directly from the residual plastic deformations after the load is removed, in nanoindentation this area is calculated from the geometry of the used tip, i.e., from the projected area of the tip A_c and the indentation depth h_c (Fig. 1) [4]. The ideal area A_c of the herein used standard Berkovich nanoindenter is given by [2-3]:

$$A_c = 24.5 \cdot {h_c}^2 \quad (1)$$

where h_c can be determined as [3]:

$$h_c = h_{max} - 0.75 \frac{P_{max}}{dP/dh} \quad (2)$$

It has to be noted that Eq. (1) is based on the assumption of an infinitely sharp indenter tip. A correction in terms of the contact depth has thus to be introduced to take into account its factual state, so that Eq. (1) is modified as [2-3]:

$$A_c = 24.5(h_c + \Delta h)^2 \quad (3)$$

where Δh represents a correction factor (cf. Fig. 1).

2.1. Experimental assessment

In the frame of this work, the nanoindentation measurements are carried on the studied (100)-oriented single crystal Si wafer by using a Keysight G200 Nanoindenter, allowing to attain load resolutions of 50 nN and displacement resolutions down to 0.01 nm [5]. A standard loading-unloading method is used in all the experiments, while the temperature in the measurement chamber is kept stable at 28 °C. E and H values are hence obtained from the slope of the resulting unloading part of the P-h curve [3]. Three different indentation depths of 50 nm, 75 nm and 100 nm are considered, and nine tests are performed at each indentation depth. In Fig. 2 is thus shown a typical experimentally obtained P-h curve at the maximum indentation depth h_{max} = 500 nm. P_{max} designates here the maximum indentation load, dP/dh is the initial slope of the unloading curve, h_{el} is the elastic recovery, while h_{pl} indicates the residual (plastically deformed) depth after complete unloading. It can be noted here that the shown P-h curve exhibits during unloading a localized perturbation (marked in the figure with A), which can be related to a phase transformation. Similar phenomena have already been observed and described in prior art [1]. In fact, the contact pressure beneath the indenter can be quite high, thus reaching the critical pressure triggering a structural transformation, hence closely matching the situation when large hydrostatic loads induce materials' phase transformations.

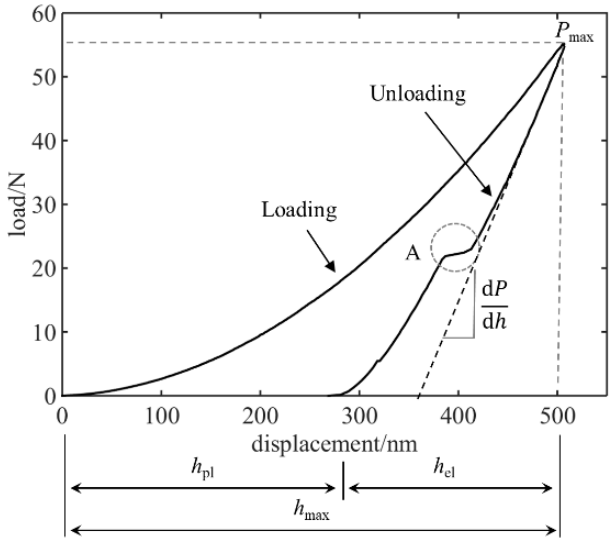

Figure 2. Typical P-h curve obtained experimentally at h_{max} = 500 nm.

In Table 1 are summarized the values of E, H and P_{max} calculated from the obtained experimental data for the three considered indentation depths. These will be used in the following numerical analyses.

Table 1. E, H and P_{max} values for different indentation depths.

h_{max}/nm	E/GPa	H/GPa	P_{max}/mN
50	199.56	15.35	0.82
75	197.58	14.33	1.68
100	187.63	13.50	2.74
Average:	194.92	14.40	-

2.2. Numerical simulations

The use of FEA to study the nanoindentation process allows understanding better the influence of the indenter, the sample geometry, the contact conditions, and the material behaviour on the obtained results. The goal is to determine a methodological procedure that allows determining a set of unique elasto-plastic material parameters that can be adopted to replicate the nanoindentation process by numerical simulations, and to do so independently of the indentation depth.

In a first instance, the nanoindentation experiment is modelled numerically as a nonlinear two dimensional (2D) axisymmetric finite element (FE) problem, while, to optimize the geometrical parameters of the model (sample radius r_s and height h_s, as well as the indenter tip radius ρ_{ind}), an elastic material behaviour is considered. The mesh is defined with a total of 10 950 three-node triangular elements with 5 585 nodes, and, to minimize the computational time while allowing to resolve the large stress and strain gradients, it is refined at the indentation site and made coarser away from it (Fig. 3). Since nanoindentation is a contact problem, a very fine mesh between the indenter and the specimen allows to determine the contact area, as well as to impose accurately the contact elements [6]. Contact itself is defined as a sliding surface without friction. The lower edge of the model is then fixed, while the symmetry boundary condition is applied along the y axis. The Berkovich indenter itself is modelled as a rigid "line". Displacement controlled loading is hence imposed on the indenter tip in all simulations. The initial geometrical and material parameters adopted in nonlinear elastic FEA are summarized in table 2 [7]. To isolate the effect of the FE model size and of indenter's tip radius on the obtained results, several simulations are hence carried on considering different values of r_s, h_s and ρ_{ind} as well as different indentation depths h_{max}.

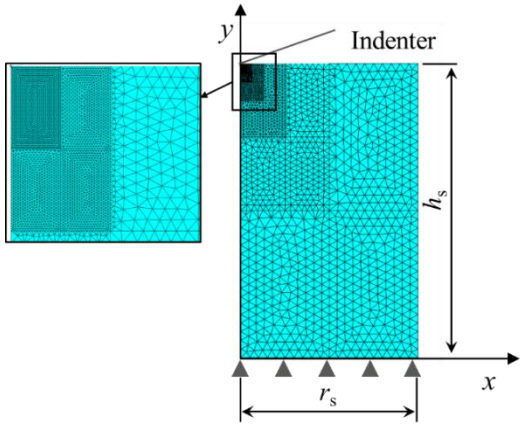

Figure 3. Axisymmetric finite element (FE) model with boundary constraints and geometrical parameters.

Table 2. Initial geometrical and material parameters of the FE model.

Angle of the Berkovich tip α/°	70.3
Correction factor β/-	1
Sample radius r_s/µm	18
Sample height h_s/µm	30
Elastic modulus of the sample E_{mat}/GPa	70
Poisson ratio of the sample ν_{mat}/-	0.3
Radius of the indenter ρ_{ind}/nm	200
Elastic modulus of the indenter E_{ind}/GPa	1000
Poisson ratio of the indenter ν_{ind}/-	0.07
Maximum depth h_{max}/nm	600

The sensitivity analyses performed with the developed FE model allow establishing that the P-h curves converge when $h_s/h_{max} \geq 100$ and $r_s/h_s \geq 1$. The latter can be observed also in Fig. 4. What is more, the attained results show a good correspondence in trends with those obtained in prior art [7].

To simulate the loading and unloading phases of the single nanoindentation test, in the following step the nonlinear numerical simulations are performed adopting the bilinear

elasto-plastic material model with kinematic hardening. The values of E and H calculated from experimental data, along with the maximum depth in each experiment, are used here as input parameters, where the E value adopted in the simulations is the average value obtained experimentally at different indentation depths (cf. table 1).

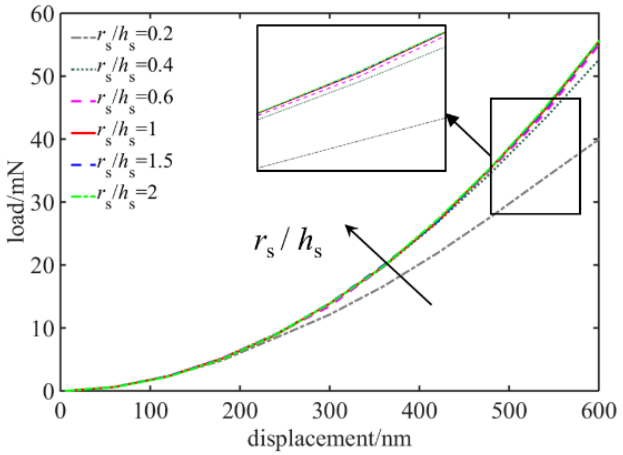

Figure 4. *P-h* curves for the elastic FEA with h_s=30 μm and varying r_s (r_s = 6, 12, 18, 30, 45 and 60 μm).

Based on the results of previous calculations ($h_s/h_{max} \geq 100$ and $r_s/h_s \geq 1$), in this stage of the study it is necessary to redefine somewhat the numerical model. After a convergence test, a mesh with a total of 4 927 eight-node quadrilateral elements and 14 724 nodes is thus adopted. As in the previous case, the mesh is refined in the indentation region. The von Mises yield criterion and the material model are then adopted considering four parameters: Young modulus's E, Poisson ratio ν, yield stress σ_0 and hardening modulus E_T. The latter defines the slope of the stress-strain curve in the plastic region, i.e., its value indicates the monotonic hardening capacity of the material.

Results of experiments reported in literature [3, 8] show that the mean pressure between the indenter and the specimen is directly proportional to the material yield stress, and can be expressed as:

$$H = C\sigma_0 \tag{4}$$

where C is the constrained factor (for metals ≈ 3). It would, hence, seem that σ_0 can be evaluated in a straightforward manner based on accurate measurements of hardness. It has been observed, however, that C is strongly dependent on the material parameters and can vary from 1.5 (for low values of the E/σ_0 ratio, e.g. for glasses) to 3 (for large E/σ_0 values, e.g. for metals) [3, 8]. Once the elasto-plastic material model is adopted, sensitivity analyses of the influence of E, σ_0, E_T and ρ_{ind} are thus performed to investigate how these parameters affect the *P-h* curve.

3. Results and discussion

It is evident that the majority of materials exhibit elasto-plastic deformations during the nanoindentation process. It is therefore quite important to establish a methodological approach to determine the elasto-plastic material properties (cf. Fig. 2). This deviates considerably from the linear elastic assumption on which the conventionally used Sneddon's relation is based [3]:

$$P = \frac{2E\tan\alpha}{\pi(1-\nu^2)}h^2 \tag{5}$$

In fact, the main assumption underlying all nanoindentation experiments is that, while the loading stage is elasto-plastic, the unloading stage is purely elastic [8]. Factors identified as relevant to linear elastic indentations, such as the finite tip radius effect, are, however, not considered in Sneddon's formulations [3]. In fact, the tip of the indenter is conventionally made of diamond or sapphire, formed into a sharp, symmetric shape, as in the case of the three-sided Berkovich pyramid used in this work. Usually the radius of a fresh nanoindenter tip is in the 30 nm … 200 nm range [8], but the tip is never atomically sharp, exhibiting a significant blunting that increases with the number of performed measurements [1]. This aspect is, thus, thoroughly studied via the developed FE model, allowing to obtain the results depicted in Fig. 5. It can be observed here that the influence of ρ_{ind} is consistent with the expectations, i.e., that a blunt tip requires a larger load than the sharp (fresh) one to penetrate to the same depth into the specimen. What is more, in FEA the tip radius may also affect the elasto-plastic transition [2].

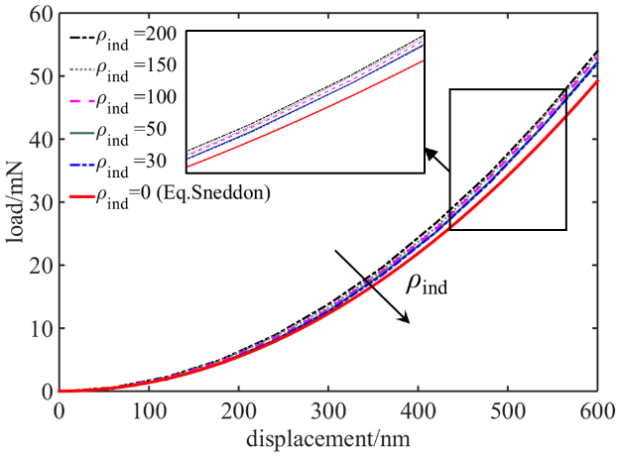

Figure 5. *P-h* curves for the elastic FEA and varying tip radii ρ_{ind}.

Because of the very fine scale of nanoindentation testing, imperfections in the pyramidal shape of the tip may also affect the obtained results. In fact, in prior art it is reported that tip rounding becomes important when the maximum depth of penetration is of the order of 50 nm [3]. Young's modulus measurements will not be affected much by tip rounding, as long as the shape of the indenter is characterized by the area function A_c. On the other hand, however, if Δh represents the truncation of the tip (cf. Fig. 1), the quantities h_{max} and h_c will be wrong by the same value – an error whose relevance will become bigger as the indentation depth h_{max} decreases [3]. In table 3 are thus reported the results of the mechanical parameters and of the corresponding errors calculated for different indentation depths. Equations (1) and (3) are adopted here to calculate the value of the hardness H for a certain value of the P/A_c ratio. It can, hence, be noted that the contact area error becomes indeed significant for small indentation depths, confirming, thus, that in the calculation of A_c it is important to take into consideration the correction factor Δh.

Table 3. E and H calculated numerically for different indentation depths, and H obtained with and w/o indentation depth correction.

h_c/nm	E/GPa	Err./%	A_c from Eq. (1)		A_c from Eq. (3)	
			H/GPa	Err./%	H/GPa	Err./%
50	163.89	1.0	23.6	96.5	13.24	10.3
75	164.33	0.8	20.4	69.7	13.76	14.7
100	166.48	0.5	18.6	55.3	13.84	15.3

As it was mentioned earlier, the majority of materials exhibits elasto-plastic deformations during the nanoindentation process. The elasto-plastic material model is thus to be adopted in FEA to address properly the material behaviour observed during the experiments. Taking into consideration the elasto-plastic material behaviour, the performed sensitivity analyses allow then establishing that the loading part of the *P-h* curve increases

in magnitude with higher E values, while the unloading part becomes steeper. Similarly, by increasing the value of the hardening modulus E_T, the unloading part tends to move upwards. On the other hand, the first part of the unloading curve remains almost unaffected, while for bigger E_T values the inclination of the last part of the curve increases (Fig. 6).

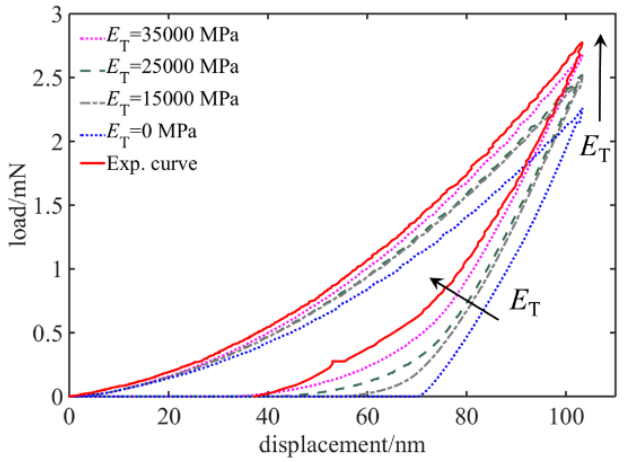

Figure 6. *P-h* curves for the elasto-plastic FEA with varying hardening modulus E_T.

The determination of the considered mechanical properties is, therefore, carried on following the methodological approach shown schematically in the flow chart depicted in Fig. 7. The experimentally obtained parameters (E, H, h_{max}, P_{max}) that remain unchanged during the calibration procedure are distinguished here from the "adjustable" parameters E_T, σ_0 and ρ_{ind}, which are tuned to fit accurately the FEA obtained curves to the experimental ones. In fact, since it is not straightforward to determine the values of the stresses and strains from the nanoindentation experiments, E_T, σ_0 and ρ_{ind} have to be iteratively varied until the best fit of the *P-h* curves is obtained.

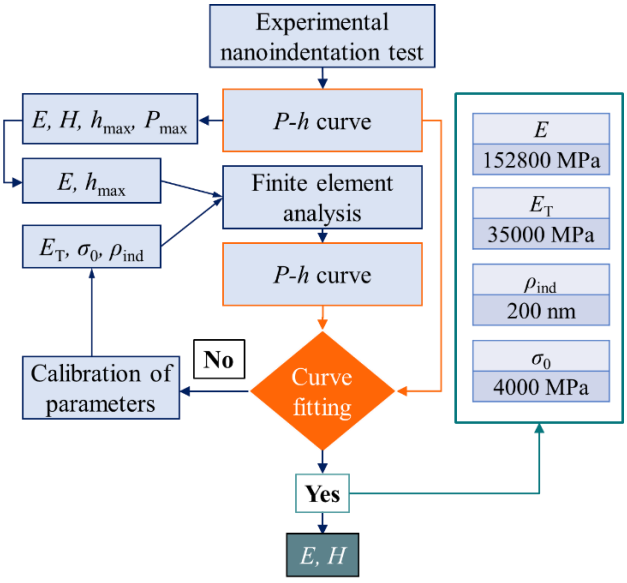

Figure 7. Calibration procedure of material parameters.

The hence determined parameters are lastly used in the final set of numerical simulations for different h_{max} values, and the thus obtained results are given in Fig. 8. It can be noted here that, by using a single set of calibrated parameters, an excellent agreement between the experimental and the FEA curves is obtained for all the considered indentation depths.

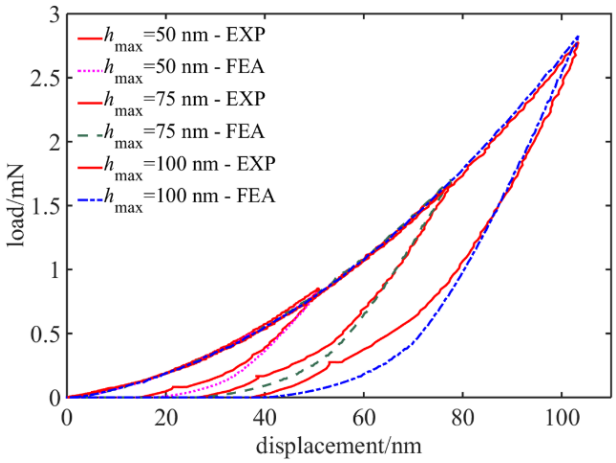

Figure 8. Comparison between experimental and FEA *P-h* curves calculated with calibrated parameters for different indentation depths.

4. Conclusions and outlook

A methodological approach is used in this work to correlate the load vs. indentation depth curves obtained experimentally via nanoindentation to those attained by an FE numerical procedure. The nanoindentation tests are conducted by using the standard Berkovich tip, whereas axisymmetric FE models are developed for the back-calculation of the elasto-plastic material parameters. The numerical simulations are conducted herein by using a bilinear elasto-plastic material model, enabling to perform sensitivity analyses of the influence of the parameters of the used material model. It is hence shown that, once the material parameters of the FEA are calibrated, they are valid for different indentation depths. In fact, the proposed procedure enables replicating the experimental curves with estimated errors lower than 1 % and 15 % for E and H, respectively. It is also established that, when evaluating numerically hardness, tip shape and radius affect significantly the accuracy of the obtained results, which is especially evident for smaller indentation depths. In that case, when calculating the effective area of the indenter tip, it is important to take into consideration the correction of the factual indentation depth.

The same approach will be applied in future work to other materials as well as to samples obtained by additive technologies in order to validate the proposed modelling approach and/or the limits of applicability of the developed models for different classes/types of materials. The developed systematic approach will be used also to investigate the material properties of thin films (e.g. aluminium oxide and titanium dioxide) deposited on a Si substrate, widely used in MEMS and NEMS technologies due to their thoroughly studied optical, electronic and biocompatible properties.

Acknowledgements

Work enabled by using the equipment funded via the EU ERDF project "RISK", and via the support of the University of Rijeka, Croatia, grants uniri-tehnic-18-32 and uniri-mladi-tehnic-20-18.

References

[1] Schuh C A 2006 *Mater. Today* **9**(5) 32-40
[2] Toress-Toress D et al. 2014 *Modelling Simul. Mater. Sci. Eng.* **18**
[3] Fischer-Cripps A C 2011 *Nanoindentation* – 3rd ed. (NY: Springer)
[4] Rice P M, Stoller R E 2000 *MRS Online Proceedings Library* 649, 711
[5] University of Rijeka, Croatia, http://nanori.uniri.hr/wp-content/uploads/2018/04/Katalog-CMNZT_ENG.pdf
[6] Lanzutti A, Srnec Novak J et al. 2020 *Eng. Fail. Anal.* **116** 104755
[7] Poon B 2009 *A critical appraisal of nanoindentation with application to elastic-plastic solids and soft materials* PhD thesis (Caltech)
[8] Poon B et al. 2008 *Int. J. Solids Struct* **45** 6399-415